

## Novel polyoxometalate silica nano-sized spheres: efficient catalysts for olefin oxidation and the deep desulfurization process†

Cite this: *Dalton Trans.*, 2014, **43**, 9518

Lucie S. Nogueira,<sup>a</sup> Susana Ribeiro,<sup>a</sup> Carlos M. Granadeiro,<sup>a</sup> Eulália Pereira,<sup>a</sup> Gabriel Feio,<sup>b</sup> Luís Cunha-Silva<sup>a</sup> and Salet S. Balula\*<sup>a</sup>

A novel method to prepare silica nano-sized particles incorporating polyoxometalates was developed leading to a new efficient heterogeneous oxidative catalyst. Zinc-substituted polyoxotungstate [PW<sub>11</sub>Zn-(H<sub>2</sub>O)O<sub>39</sub>]<sup>5-</sup> (PW<sub>11</sub>Zn) was encapsulated into silica nanoparticles using a cross-linked organic–inorganic core, performed through successive spontaneous reactions in water. The potassium salt of PW<sub>11</sub>Zn and the composite formed, PW<sub>11</sub>Zn-APTES@SiO<sub>2</sub>, were characterized by a myriad of solid-state methods such as FT-IR, FT-Raman, <sup>31</sup>P and <sup>13</sup>C CP/MAS solid-state NMR, elemental analysis and SEM-EDS, confirming the integrity of the PW<sub>11</sub>Zn structure immobilized in the silica nanoparticles. The new composite has shown to be a versatile catalyst for the oxidation of olefins and also to catalyze the desulfurization of a model oil using H<sub>2</sub>O<sub>2</sub> as the oxidant and acetonitrile as the solvent. The novel composite material was capable of being recycled without significant loss of activity and maintaining its structural stability for consecutive desulfurization and olefin oxidative cycles.

Received 7th December 2013,  
Accepted 3rd April 2014

DOI: 10.1039/c3dt53444h

www.rsc.org/dalton

### Introduction

The design of novel heterogeneous catalysts easily recyclable without a loss of activity and selectivity is a challenging goal of liquid phase oxidation catalysis. The development of eco-sustainable catalytic systems to transform cheap compounds into valuable intermediates for organic synthesis is an area of interest for both the laboratory and industry. Polyoxometalates (POMs) are a class of well-defined early transition metal oxygen clusters, which exhibit distinctive structures and various functionalities.<sup>1</sup> POMs have received increasing attention as oxidative catalysts due to a unique combination of properties, including thermal and oxidative stability, tuneable acidity, redox potentials, solubility, *etc.*<sup>1–3</sup> Transition-metal mono-substituted polyoxotungstates contain an active center M isolated in the tungsten oxide matrix and strongly bound through M–O–W bridges, which may confer an additional catalytic activity for oxidative reactions and a high capacity as oxygen transfer agents.<sup>2,4</sup> These compounds have shown to be

economical and environmentally attractive oxidation catalysts in both research and industrial processes.<sup>5</sup> Hydrogen peroxide is one of the most attractive oxidants, mainly because it is environmentally clean and easily handled.<sup>6</sup> Recently, remarkable interest has been noticed for the application of heterogeneous catalyst based POMs in the oxidation of various valuable molecules (alkenes, alkanes, alcohols and sulfides) in the presence of H<sub>2</sub>O<sub>2</sub>, mainly due to the necessity of recovering and recycling these active catalytic compounds. Different methodologies have been studied using silica as a solid support to immobilize POMs *via* dative, covalent or electrostatic binding.<sup>1,7–17</sup> One of the most widely used immobilization strategies is electrostatic bonding to NH<sub>2</sub>-modified mesoporous silica or to imidazolium ionic liquid immobilized on silica. In both cases the POM is linked *via* anion exchange or formation of ion pairs.<sup>17,18</sup> Furthermore, some heterogeneous POM based silica catalysts have been prepared by immobilization of POMs through electrostatic interaction with the surface of positively charged silica nanoparticles.<sup>19–21</sup> Another well-known strategy is the encapsulation of POMs into core/silica nanoparticles using a reverse micelle and sol–gel technique.<sup>22–25</sup> In particular, the sol–gel method is a promising approach to heterogenize POMs through occlusion of the POM into an inert matrix. Immobilization of POMs by surfactant encapsulation has also been recently explored to form supramolecular hybrid catalysts by replacement of the counter cations from the POMs by quaternary ammonium cations,

<sup>a</sup>REQUIMTE & Departamento de Química e Bioquímica, Faculdade de Ciências, Universidade do Porto, 4169-007 Porto, Portugal. E-mail: sbalula@fc.up.pt; Tel: +351 220 402 576

<sup>b</sup>CENIMAT/I3N, Departamento de Ciência dos Materiais, Faculdade de Ciências e Tecnologia, Universidade Nova de Lisboa, 2829-516 Monte da Caparica, Portugal

† Electronic supplementary information (ESI) available. See DOI: 10.1039/c3dt53444h

such as di-(11-hydroxyundecyl)dimethylammonium (DOHDA).<sup>26,27</sup> In general, diffusion restriction of the POM within the silica matrix seems to be crucial to prevent POM leaching into solution.

In a sequence of our recent studies concerning the preparation of heterogeneous catalysts by incorporation of POMs into distinct solid supports,<sup>15–17,28–30</sup> we proposed a new methodology to prepare POM based silica composites *in situ* in a cross-linked organic/inorganic hybrid core in an effort to establish a facile strategy to prepare uniform and well dispersed POMs inside silica spheres. The catalytic core is formed by the mono-substituted  $[\text{PW}_{11}\text{Zn}(\text{H}_2\text{O})\text{O}_{39}]^{5-}$  ( $\text{PW}_{11}\text{Zn}$ ) linked to the amine-organosilane (APTES) surrounded by a silica shell (Fig. S1 in ESI†). The resulting composite,  $\text{PW}_{11}\text{Zn-APTES@SiO}_2$ , is expected to combine the advantages of molecular complexes and reusable solids. The  $\text{PW}_{11}\text{Zn}$  was judiciously chosen because the application of this POM as a catalyst for oxidative systems remains practically unexplored. There is only one published example of the use of  $\text{PW}_{11}\text{Zn}$  as a homogeneous catalyst for the oxidation of alcohols<sup>31</sup> and, to our knowledge, only one other report describes the immobilization of  $\text{PW}_{11}\text{Zn}$  in a silica support material, although anchored on the surface of amorphous silica.<sup>32</sup> The composite particles of  $\text{PW}_{11}\text{Zn-APTES@SiO}_2$  were tested as a heterogeneous catalyst in two different catalytic systems using  $\text{H}_2\text{O}_2$  as an oxidant. The oxidation and epoxidation of olefins originate oxygenated products of great interest.<sup>33</sup> The second catalytic system consists in its application in oxidative desulfurization systems (ODS). In fact, the development of efficient ODS systems is crucial for the production of ultra low levels of sulfur fuels and, in general, POMs have shown to be efficient catalysts for oxidative desulfurization.<sup>29,30,34–36</sup> However, the application of POM based silica composites as heterogeneous catalysts has been poorly explored for the ODS technology.<sup>36,37</sup>

## Experimental section

### Materials and methods

All the reagents used in the preparation of the POMs and the silica composites, namely sodium tungstate dihydrate (Aldrich), sodium hydrogen phosphate dihydrate (Aldrich), zinc acetate dihydrate (May & Baker), nitric acid 65% (Merck), potassium chloride (Aldrich), ethanol (Aga), tetraethoxysilane (TEOS, Aldrich), (3-aminopropyl)triethoxysilane (APTES, Aldrich) and ammonia 25% (Merck), were used as received. Geraniol 98% (Aldrich), *cis*-cyclooctene 95% (Aldrich), styrene 98% (Aldrich), dibenzothiophene 99% (Aldrich), 4,6-dimethyldibenzothiophene 98% (Aldrich), acetonitrile (MeCN, Panreac), and hydrogen peroxide 30% (Riedel-de-Häen) were purchased from commercial suppliers and used without further purification. Elemental analyses were performed by ICP-MS on a Varian 820-MS at the University of Santiago de Compostela. Infrared absorption spectra were recorded on a Jasco 460 91 Plus using KBr pellets, while the FT-Raman spectra were recorded on a RFS-100 Bruker FT-spectrometer

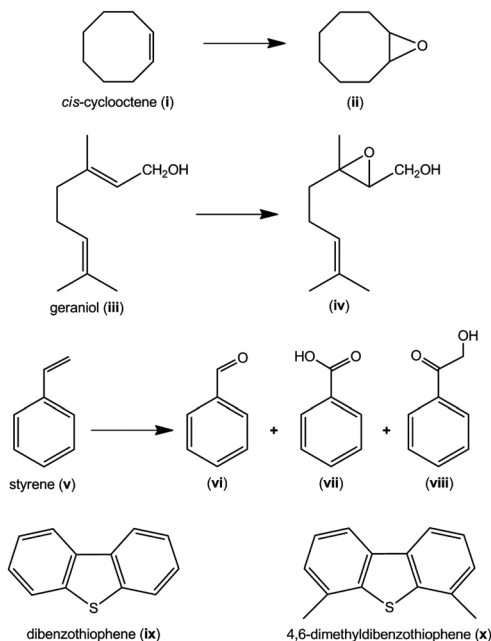
equipped with a Nd:YAG laser with an excitation wavelength of 1064 nm and the laser power set to 350 mW. Electronic absorption spectra were acquired on a Varian Cary 50 Bio spectrophotometer. <sup>31</sup>P NMR spectra were recorded on a Bruker Avance III 400 using  $\text{CD}_3\text{CN}$  as the solvent and the chemical shifts are given relative to 85%  $\text{H}_3\text{PO}_4$  as an external standard. Solid-state <sup>31</sup>P MAS NMR spectra were acquired with a 7 T (300 MHz) AVANCE III Bruker spectrometer under a magic angle spinning of 10 kHz at room temperature. The spectra were obtained by a solid echo sequence with an echo delay of 15  $\mu\text{s}$ , a 90° pulse of 10.5  $\mu\text{s}$  at a power of 20 W, and a relaxation delay of 30 s. Potassium phosphate ( $\text{K}_3\text{PO}_4$ ) was used as a reference. Scanning electron microscopy (SEM) and energy dispersive X-ray spectroscopy (EDS) studies were performed at “Centro de Materiais da Universidade do Porto” (CEMUP, Porto, Portugal) using a scanning electron microscope JEOL JSM 6301F operating at 15 kV equipped with an energy-dispersive X-ray spectrometer Oxford INCA Energy 350. The samples were studied as powders and were subjected to gold sputtering before analysis. The catalytic reactions were monitored by GC-FID performed in a Bruker 430-GC. Hydrogen was used as the carrier gas (55  $\text{cm}^3 \text{s}^{-1}$ ) and fused silica Supelco capillary columns SPB-5 (30 m  $\times$  0.25 mm i.d.; 25  $\mu\text{m}$  film thickness) were used.

### Synthesis and preparation of materials

**Zinc-substituted polyoxotungstate.** The potassium salt of  $[\text{PW}_{11}\text{Zn}(\text{H}_2\text{O})\text{O}_{39}]^{5-}$  ( $\text{PW}_{11}\text{Zn}$ ) was prepared according to a previously described procedure.<sup>38</sup> The POM was characterized by UV-Vis spectroscopy, vibrational spectroscopy (FT-IR and FT-Raman) and <sup>31</sup>P NMR spectroscopy that allowed to positively confirm the identity of the compound.

**$\text{PW}_{11}\text{Zn-APTES@SiO}_2$  nanospheres.** The silica nanoparticles were prepared by adding a solution containing APTES (0.64 mmol) to a solution of  $\text{PW}_{11}\text{Zn}$  (0.054 mmol) in water (10 mL). The mixture was then kept under stirring at room temperature for 2 h. Then, ethanol (8.75 mL), TEOS (1.2 mmol) and ammonia (1.5 mL) were slowly added under stirring to the initial suspension. After stirring for 24 h at room temperature, the mixture was centrifuged and the silica composites were washed thoroughly with an ethanol–water 1 : 1 solution and dried in a desiccator over silica gel.  $\text{PW}_{11}\text{Zn-APTES@SiO}_2$ : Anal. found (%): W, 20.1; C, 9.3; N, 2.6; loading of  $\text{PW}_{11}\text{Zn}$ : 0.099 mmol per 1 g and ratio of APTES/ $\text{PW}_{11}\text{Zn}$  = 19. Selected FT-IR ( $\text{cm}^{-1}$ ): 3412, 2925, 1644, 1338, 1132, 1044, 944, 904, 798, 770, 690, 668, 618, 584, 574, 560, 542, 438. Selected FT-Raman ( $\text{cm}^{-1}$ ): 3302, 2918, 1607, 1454, 1412, 1310, 1231, 1142, 1048, 978, 959, 857, 754, 587, 500, 434.

**Catalytic olefin oxidations.** The oxidation reactions of *cis*-cyclooctene (i), geraniol (iii) and styrene (v) (Scheme 1) were carried out in MeCN, in a borosilicate 5 mL reaction vessel, with addition of aqueous  $\text{H}_2\text{O}_2$  (30 wt%), in the presence of potassium salt of the zinc-substituted POM ( $\text{PW}_{11}\text{Zn}$ ) or the composite  $\text{PW}_{11}\text{Zn-APTES@SiO}_2$ . The oxidation of geraniol was studied at room temperature and protected from light, whereas the oxidative reactions of *cis*-cyclooctene and styrene were studied at 70 °C. In a typical experiment, the catalyst



**Scheme 1** Chemical structure of the substrates investigated and their respective oxidation products.

(3  $\mu\text{mol}$  of  $\text{PW}_{11}\text{Zn}$  or 30 mg of  $\text{PW}_{11}\text{Zn-APTES@SiO}_2$ ) was added to 1 mmol of the substrate in MeCN (1.5 mL) under stirring. The reaction was started by addition of  $\text{H}_2\text{O}_2$  to the reaction mixture, 4.5 mmol for the oxidation of (iii) and (v) and 1 mmol for the oxidation of (i). The reactions were followed by GC analysis and stopped when a complete conversion of the substrate was observed or when the product yields remained constant after two successive GC analyses. At regular intervals, an aliquot was taken directly from the reaction mixture with a microsyringe, diluted in MeCN, centrifuged (when necessary) and injected into the GC or GC-MS equipment for analysis of starting materials and products. When the composite catalyst was used, it was filtered off at the end of reactions, and washed with MeCN several times to remove the remaining substrate, reaction products and the oxidant. The recovered catalyst was dried at room temperature overnight and reused in a new reaction under identical experimental conditions, with readjustment of all quantities, without changing the molar ratios and reaction concentrations. Blank reactions were performed for all substrates, confirming that no oxidation products are obtained unless the catalyst and  $\text{H}_2\text{O}_2$  are present.

**Catalytic oxidative desulfurization process (ODS).** The oxidative desulfurization studies were performed using a model oil containing dibenzothiophene (DBT, ix in Scheme 1) and 4,6-dimethyldibenzothiophene (4,6-DMDBT, x in Scheme 1) in *n*-octane as the representative refractory sulfur-compounds in diesel. The ODS experiments were carried out under air (atmospheric pressure) in a closed borosilicate 5 mL reaction vessel equipped with a magnetic stirrer and immersed in a thermostatically controlled liquid paraffin bath at 50  $^\circ\text{C}$ . The ODS studies were performed using the heterogeneous catalyst  $\text{PW}_{11}\text{Zn-APTES@SiO}_2$  in a biphasic system formed by the

model oil and MeCN. In a typical catalytic reaction, 30 mg of  $\text{PW}_{11}\text{Zn-APTES@SiO}_2$  (containing the equivalent of 3  $\mu\text{mol}$  of  $\text{PW}_{11}\text{Zn}$ ) were added to 0.75 mL of MeCN and 0.75 mL of the model oil. This mixture was stirred for 10 min until the initial extraction equilibrium was reached. An aliquot from the upper oil phase was taken. The catalytic reaction was initiated by the addition of the oxidant  $\text{H}_2\text{O}_2$  (75  $\mu\text{L}$ ). The DBT and the 4,6-DMDBT contents in the model oil were quantified periodically by GC analysis using tetradecane as a standard. At the end of each ODS process the heterogeneous catalyst  $\text{PW}_{11}\text{Zn-APTES@SiO}_2$  was recovered by filtration, washed several times with MeCN, dried at room temperature overnight and then reused in a new ODS cycle under the same reaction conditions as before.

## Results and discussion

### Catalyst characterization

The  $\text{PW}_{11}\text{Zn-APTES@SiO}_2$  composite was prepared through the initial formation of a cross-linked organic/inorganic hybrid core and the subsequent formation of a silica shell by the alkaline hydrolysis of TEOS. The POM-containing silica spheres were characterized by several characterization techniques including vibrational spectroscopy (FT-IR and FT-Raman), solid-state  $^{31}\text{P}$  and  $^{13}\text{C}$  CP/MAS NMR spectroscopy, elemental analysis, scanning electron microscopy (SEM) and energy dispersive X-ray spectroscopy (EDS). The vibrational spectroscopy data of the composite material are shown in Fig. 1. The FT-IR spectrum of  $\text{PW}_{11}\text{Zn-APTES@SiO}_2$  exhibits the main bands associated with the silica framework stretches, namely the intense band located at 1044  $\text{cm}^{-1}$  assigned to the  $\nu_{\text{as}}(\text{Si-O-Si})$  stretch, as well as the  $\nu_{\text{as}}(\text{Si-OH})$ ,  $\nu_{\text{s}}(\text{Si-O-Si})$  and  $\delta(\text{Si-O-Si})$  stretching modes located at 944, 798 and 438  $\text{cm}^{-1}$ , respectively.<sup>39,40</sup> These intense bands mask some of the bands associated with the zinc phosphotungstate vibrational modes. Nevertheless, comparing the spectrum of the composite with the typical bands of silica frameworks, it is possible to observe the presence of two bands located at 904 (sh.) and 770  $\text{cm}^{-1}$  that should correspond to the  $\nu_{\text{as}}(\text{W-O}_b\text{-O})$  and  $\nu_{\text{as}}(\text{W-O}_c\text{-O})$  stretches of the POM, respectively.<sup>39,41</sup> The presence of the POM in the composite is more evident in the FT-Raman spectrum since the intense silica bands that overlap and mask the POM bands in FT-IR are less active in Raman.<sup>24</sup> The FT-Raman spectrum of the  $\text{PW}_{11}\text{Zn-APTES@SiO}_2$  is mainly composed by some of the typical POM stretching modes, namely the  $\nu_{\text{as}}(\text{P-O}_a)$ ,  $\nu_{\text{as}}(\text{W-O}_d)$ ,  $\nu_{\text{s}}(\text{W-O}_d)$  and  $\nu_{\text{as}}(\text{W-O}_b\text{-O})$  vibrations located at 1048, 978, 959 and 857  $\text{cm}^{-1}$ , respectively.<sup>15,41</sup> A small shift to lower wavelengths relative to the isolated POM is observed, especially in the bands assigned to the  $\nu(\text{W-O}_d)$  stretches, probably due to the interaction between the POM and the support as previously reported.<sup>17,42</sup> The FT-Raman spectrum also exhibits some bands assigned to the APTES modes, including a broad band located at approximately 2918  $\text{cm}^{-1}$  assigned to the  $\nu_{\text{as}}(\text{C-H})$  and  $\nu_{\text{s}}(\text{C-H})$  stretching, the bands at 1454 and 1412  $\text{cm}^{-1}$  arising from the  $\text{CH}_2$  scissor-

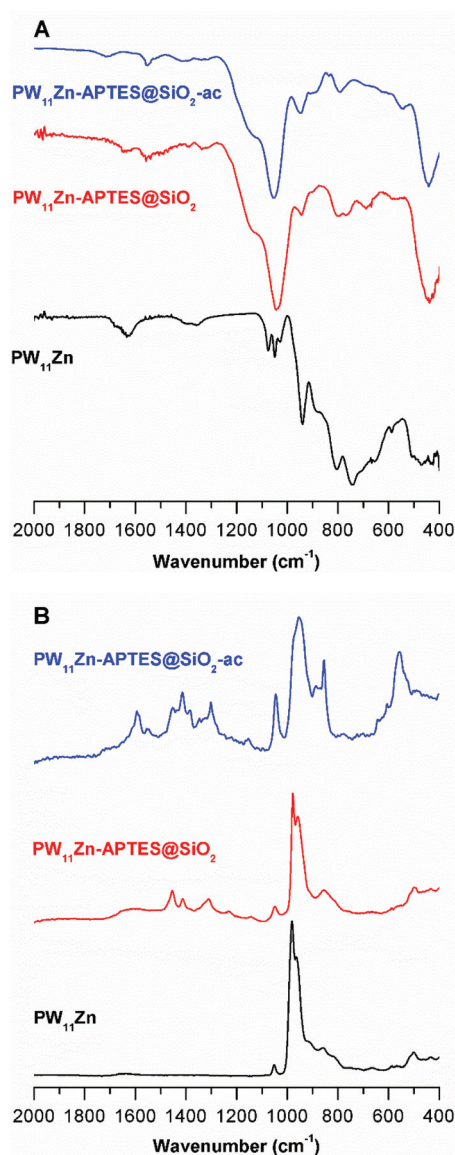


**Fig. 1** FT-IR (A) and FT-Raman (B) of  $PW_{11}Zn$ , and the POM-containing silica nanospheres before,  $PW_{11}Zn-APTES@SiO_2$ , and after catalysis (ac),  $PW_{11}Zn-APTES@SiO_2-ac$ .

ing and CN stretch, respectively, and a band at  $1310\text{ cm}^{-1}$  from the  $\nu(C-C)$  stretching.<sup>43,44</sup> The vibrational spectroscopy results obtained for the  $PW_{11}Zn-APTES@SiO_2$  composite are in good agreement with the values described in the literature for transition-metal substituted POMs immobilized in silica matrices.<sup>17,32</sup>

The amount of  $PW_{11}Zn$  per gram of composite (0.099 mmol) was quantified by elementary analysis. The amount of APTES was also calculated to be 1.9 mmol, which indicates the presence of a large excess of APTES compared with  $PW_{11}Zn$  in the hybrid core of silica particles (ratio APTES/ $PW_{11}Zn = 19$ ). The presence and structural integrity of the POM in the silica matrix were also evaluated by  $^{31}P$  solid-state NMR spectroscopy. Fig. 2 shows the  $^{31}P$  MAS NMR spectra of

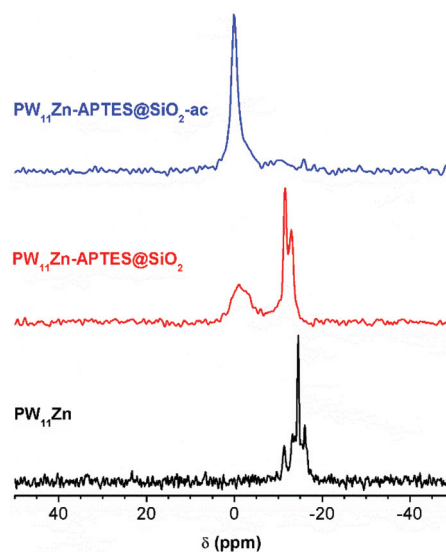


**Fig. 2**  $^{31}P$  MAS NMR spectra of  $PW_{11}Zn$ , and the silica-based composite before,  $PW_{11}Zn-APTES@SiO_2$ , and after catalysis,  $PW_{11}Zn-APTES@SiO_2-ac$ .

$PW_{11}Zn$  and  $PW_{11}Zn-APTES@SiO_2$  composites. The spectrum of  $PW_{11}Zn$  exhibits a main peak at  $-14.55$  ppm and two smaller peaks at  $-13.25$  and  $-16.02$  ppm. The main peak is assigned to the  $PW_{11}Zn$  units while the smaller ones may result from different degrees of hydration of the same units since the  $^{31}P$  MAS NMR signals of heteropolyanions are known to be very sensitive to the hydration effect.<sup>45,46</sup> A fourth peak is also observed in the spectrum ( $\delta = -11.40$  ppm) with an even smaller intensity than the previous ones and that should correspond to a small amount of  $[PW_{11}O_{39}]^{7-}$  anions formed during the synthesis of  $PW_{11}Zn$ .<sup>15,47</sup>

After the incorporation into the silica matrix, the  $^{31}P$  MAS NMR studies indicate that  $PW_{11}Zn$  is distributed over two different environments, one with the two typical peaks at  $-11.55$  and  $-13.00$  ppm (similar to free  $PW_{11}Zn$ ) and a second environment with a broad peak centred at  $-1.05$  ppm. The latter peak is typical of silica-supported Keggin-type phosphometalate anions.<sup>32,45,46,48</sup> The down-field shift relative to isolated POMs is a result of the deshielding effect on the phosphorus atoms.<sup>46</sup> The broadness of the peak is due to the different orientations of  $PW_{11}Zn$  units within the silica matrix, leading to slightly different environments around the phosphorus atoms and a larger dispersion of the  $^{31}P$  signal. Moreover, integration of  $^{31}P$  signals shows that the support-interacting  $PW_{11}Zn$  units are the predominant species in the composite material.

The  $PW_{11}Zn-APTES@SiO_2$  composite was also studied by  $^{13}C$  CP/MAS NMR spectroscopy. The spectrum of the composite before catalytic use (Fig. 3) exhibits three peaks located at 43, 22 and 10 ppm. The peaks are assigned to the C3, C2 and C1 carbon atoms, respectively, of the aminopropyl group,<sup>49</sup> and indicate that these groups remain intact in the final composite material.<sup>50</sup> Moreover, the absence of  $^{13}C$  signals from the ethoxy carbons (*ca.* 18 and 60 ppm) points to the practi-

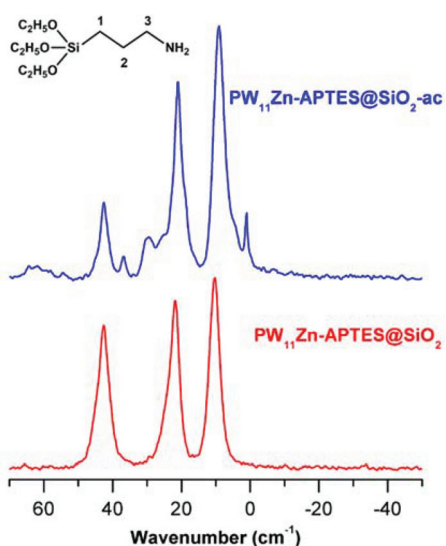


Fig. 3  $^{13}\text{C}$  CP/MAS NMR spectra of the  $\text{PW}_{11}\text{Zn-APTES@SiO}_2$  before and after catalysis (ac); the inset shows the chemical structure of APTES with carbon numbering of the aminopropyl group.

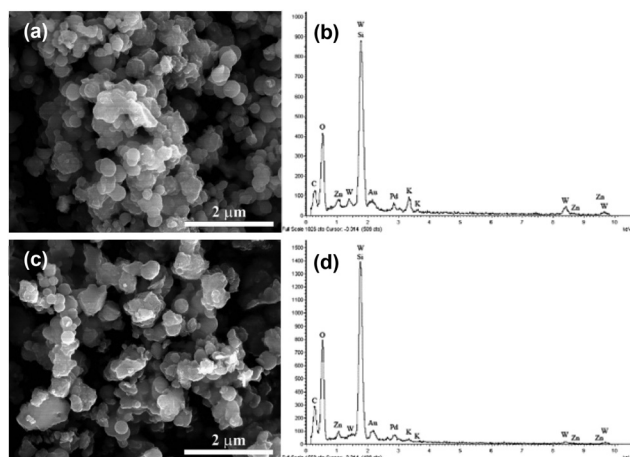


Fig. 4 SEM images of  $\text{PW}_{11}\text{Zn-APTES@SiO}_2$  (a) before and (c) after catalysis and the corresponding EDS spectra (b, d).

cally complete hydrolysis and/or condensation reactions of APTES.<sup>50,51</sup> The  $^{13}\text{C}$  CP/MAS results are in good agreement with the values reported in the literature for APTES in siliceous supports.<sup>52</sup>

The morphology and chemical composition of the  $\text{PW}_{11}\text{Zn-APTES@SiO}_2$  were studied by scanning electron microscopy (SEM) and energy dispersive X-ray spectroscopy (EDS). SEM images (Fig. 4) show that the composite material is composed of uniformly dispersed silica nanospheres with approximately 350 nm diameter, and EDS confirms the presence of  $\text{PW}_{11}\text{Zn}$  in the silica nanospheres. In addition to the intense peak of silicon, the EDS spectrum clearly indicates the presence of phosphorus, tungsten and zinc that constitute the POM.

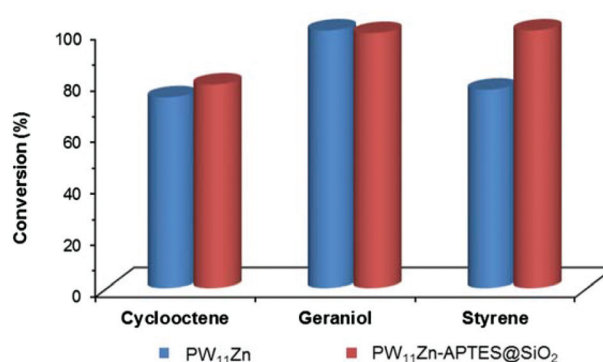
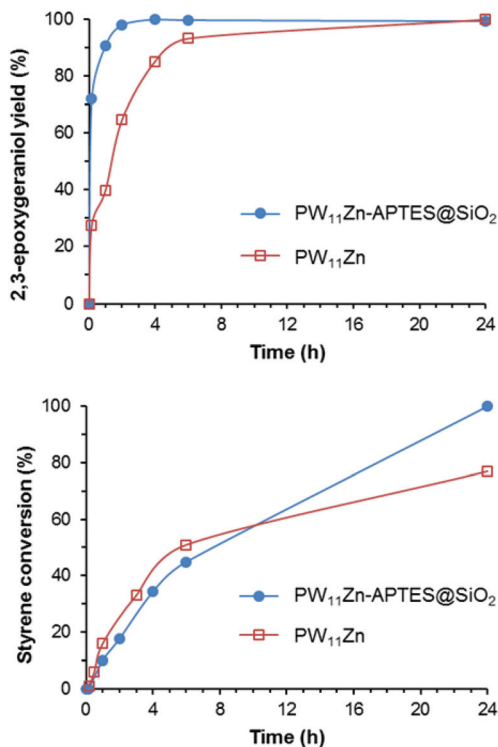


Fig. 5 Conversion data obtained for the oxidation of different substrates after 24 h of reaction using the homogeneous  $\text{PW}_{11}\text{Zn}$  and the heterogeneous  $\text{PW}_{11}\text{Zn-APTES@SiO}_2$  catalysts.

### Catalytic olefin oxidation

The oxidation of cyclooctene (i), geraniol (iii) and styrene (v) was performed using the heterogeneous catalyst  $\text{PW}_{11}\text{Zn-APTES@SiO}_2$  that was prepared by the immobilization of the active center  $\text{PW}_{11}\text{Zn}$  using a cross-linked organic-inorganic core (the organosilane APTES and the POM  $\text{PW}_{11}\text{Zn}$ ). The catalytic studies were carried out with  $\text{H}_2\text{O}_2$  as the oxidant and MeCN as the solvent. In the absence of a catalyst there was no conversion for the oxidation of the substrates studied.

The three distinct substrates were selected to evaluate the catalytic performance of the new composite  $\text{PW}_{11}\text{Zn-APTES@SiO}_2$  and its efficiency was compared with the homogeneous catalyst  $\text{PW}_{11}\text{Zn}$ . Fig. 5 displays the conversion data obtained for the oxidation of the various substrates after 24 h. It can be observed that the heterogeneous  $\text{PW}_{11}\text{Zn-APTES@SiO}_2$  presents a similar or even higher catalytic activity than the homogeneous  $\text{PW}_{11}\text{Zn}$ . Furthermore, the kinetic profiles of the homogeneous and heterogeneous catalysts were compared and are presented in Fig. S2 of ESI† for the oxidation of cyclooctene and in Fig. 6 for the oxidation of geraniol and styrene. A complete conversion was achieved in the presence of the composite after 24 h of reaction for the oxidation of styrene and geraniol. It is possible to observe that for geraniol oxidation the composite shows a better activity from the first minutes of reaction. In fact, after 10 min the conversion for geraniol oxidation was 72% in the presence of the composite and 27% in the presence of the homogeneous  $\text{PW}_{11}\text{Zn}$ . Only after 6 h of reaction, similar conversion data were achieved using the  $\text{PW}_{11}\text{Zn}$  and the composite (93% for  $\text{PW}_{11}\text{Zn}$  and 99% for the composite). The kinetic profiles for styrene oxidation (Fig. 6) demonstrate that the catalytic activity between  $\text{PW}_{11}\text{Zn}$  and the composite  $\text{PW}_{11}\text{Zn-APTES@SiO}_2$  is similar in the first 6 h of reaction and a significant superior conversion was achieved using the heterogeneous catalyst after 24 h (100% for the composite and 77% using the homogeneous  $\text{PW}_{11}\text{Zn}$ ). The increased catalytic activity found for the composite compared with the homogeneous  $\text{PW}_{11}\text{Zn}$  in the presence of an excess of the  $\text{H}_2\text{O}_2$  oxidant is probably due to the higher stability of the



**Fig. 6** Comparison of kinetic profiles for the oxidation of geraniol (top) and styrene (bottom), between the homogeneous (open symbols) and heterogeneous (solid symbols) catalysts, using  $\text{H}_2\text{O}_2$  as the oxidant and MeCN as the solvent.

active center  $\text{PW}_{11}\text{Zn}$  promoted by its encapsulation in silica nanoparticles. For the oxidation of cyclooctene an equal molar amount of substrate/oxidant was used, and in this case a similar activity between homogeneous and heterogeneous catalysts was only achieved after 24 h (79% for the composite and 74% for  $\text{PW}_{11}\text{Zn}$ , Fig. S2 in ESI†) and only 1,2-epoxycyclooctane (**ii** in Scheme 1) was formed. The stability of the homogeneous  $\text{PW}_{11}\text{Zn}$  at the end of the reaction was investigated by  $^{31}\text{P}$  NMR, and two single peaks were found at 4.3 and  $-10.5$  ppm (Fig. S3 in ESI†). The peak at  $-10.5$  ppm corresponds to  $\text{PW}_{11}\text{Zn}$  in  $\text{CD}_3\text{CN}$  solution as presented in Fig. S3† and the peak at 4.3 ppm could be identified as the Venturello complex by comparison with literature data.<sup>53,54</sup> This last peroxocomplex must be the catalytically active species.

Geraniol (**iii**) is an allylic alcohol that offers several possible positions for oxidative attack, namely at the two double bonds, at the allylic carbon centers and at the carbon of the  $\text{CH}_2\text{OH}$  group. However, the oxidation of this substrate catalyzed by  $\text{PW}_{11}\text{Zn}$  and the composite with  $\text{H}_2\text{O}_2$  at room temperature only forms the 2,3-epoxygeraniol (**iv** in Scheme 1). Few recent studies have been published reporting the epoxidation of geraniol using similar experimental conditions to this work, by various heterogeneous catalysts based on POMs immobilized onto mesoporous silica materials functionalized with amine groups.<sup>15,17</sup> In these cases, complete epoxidation of geraniol was achieved only after 24 h of reaction for the best catalysts, and in the presence of mono-substituted silicotungstates,

**Table 1** The selectivity of the various products obtained from styrene oxidation catalyzed by  $\text{PW}_{11}\text{Zn}$  and  $\text{PW}_{11}\text{Zn-APTES@SiO}_2$  after 24 h of reaction

	Selectivity (%)			Conversion (%)
	vi	vii	viii	
$\text{PW}_{11}\text{Zn}$	80	0	20	20
$\text{PW}_{11}\text{Zn-APTES@SiO}_2$				
1st cycle	54	31	15	100
2nd cycle	75	11	14	67
3rd cycle	71	21	8	96

induction periods of several hours were found. Higher catalytic performance was obtained using iron-substituted phosphotungstates encapsulated into silica nanoparticles, and in this case 96% of conversion was achieved after 3 h of reaction; however, three different products were produced.<sup>25</sup> Most of the work that has been published about the oxidation of geraniol catalyzed by Keggin type POMs was for homogeneous systems. For metal mono-substituted phosphotungstates and borotungstate selective oxidation of geraniol to 2,3-epoxygeraniol was reported under similar experimental conditions to those used in this work.<sup>14,25,55</sup> However, in the presence of the  $\text{PW}_{11}\text{Zn-APTES@SiO}_2$  catalyst, better catalytic performance and higher selectivity were obtained for less reaction time.

For styrene oxidation catalyzed by the homogeneous  $\text{PW}_{11}\text{Zn}$  or the composite  $\text{PW}_{11}\text{Zn-APTES@SiO}_2$ , the only product formed in the first 6 h of reaction was the benzaldehyde (**vi** in Scheme 1); however, after 24 h, 2-hydroxy-1-phenylethanone (**viii**) was also formed in the presence of both catalysts. In addition, using the composite, benzoic acid (**vii**) was also formed in a minor amount. Table 1 shows the product distribution and the catalytic performance obtained for styrene oxidation after 24 h of reaction in the presence of the homogeneous and heterogeneous catalysts. The oxidation of styrene to benzaldehyde with  $\text{H}_2\text{O}_2$  catalyzed by polyoxotungstates is already well documented in the literature.<sup>56–59</sup> The mechanism proceeds initially by the interaction of  $\text{H}_2\text{O}_2$  with the POM, generating active species, which may be hydroperoxo or bridging peroxo species. Then, styrene binds to one of the metal-peroxo bonds to produce a peroxometalocycle, and in the next step styrene oxide is formed. A further nucleophilic attack of  $\text{H}_2\text{O}_2$  on the styrene oxide originates benzaldehyde.<sup>56,58</sup> The formation of benzoic acid from oxidation of benzaldehyde is well documented.<sup>60</sup> Recently, our research group also observed the formation of 2-hydroxy-1-phenylethanone under similar experimental conditions, and it was confirmed that it originated from the oxidation of styrene oxide. The formation of styrene oxide was not observed in the present work probably due to its fast oxidation in the presence of an excess of  $\text{H}_2\text{O}_2$ .<sup>61</sup> Some reports can be found in the literature for the oxidation of styrene using heterogeneous catalysts based on POMs immobilized in solid supports.<sup>11,56,62–65</sup> Hu *et al.* reported the preparation of heterogeneous catalysts obtained through the impregnation of transition metal-mono-

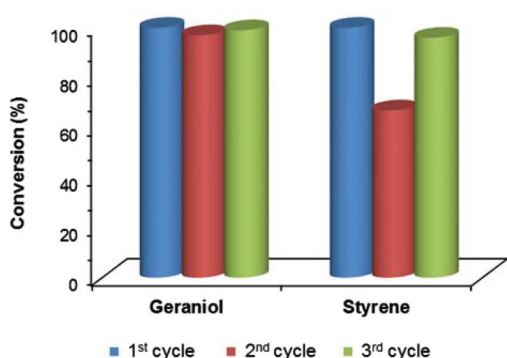


Fig. 7 Activity data obtained for the oxidation of geraniol and styrene after 24 h of reaction when catalysed by the heterogeneous  $\text{PW}_{11}\text{Zn-APTES@SiO}_2$  for three consecutive cycles.

substituted Keggin-type POMs ( $\text{XW}_{11}\text{O}_{39}$ ; X = P, Si and M = Co, Ni, Cu, Mn) in Schiff-base modified SBA-15.<sup>56</sup> The oxidation of styrene was also performed with  $\text{H}_2\text{O}_2$  as the oxidant and MeCN as the solvent, although the highest conversion value was only 57% after 12 h of reaction, significantly lower than the catalytic results presented in this work. Patel and co-workers described the catalytic oxidation of styrene in the presence of zirconia-supported POMs, in which, despite a complete conversion of styrene, the necessary reaction times are much longer than those found in the present work.

The recyclability of  $\text{PW}_{11}\text{Zn-APTES@SiO}_2$  was studied for the cases where the heterogeneous catalyst showed a similar or even higher performance than the homogeneous  $\text{PW}_{11}\text{Zn}$ , *i.e.* geraniol and styrene oxidation. The composite was recovered from the reaction mixture by centrifugation, washed several times with MeCN and dried at room temperature to be used in a fresh reaction under identical experimental conditions (using the same ratio of catalyst : substrate : oxidant : solvent). Fig. 7 shows the reusability of the composite for the oxidation of both substrates. For the oxidation of geraniol no loss of activity was noticed between the consecutive cycles. For styrene oxidation, a small decrease of activity was noticed from the first to the second cycle; however, the activity is then enhanced for the third cycle. Some differences of selectivity for the various products formed could also be observed between the different catalytic cycles (Table 1). Higher selectivity for benzaldehyde is achieved during the second and the third cycle.

### Oxidative desulfurization process (ODS)

The efficiency of  $\text{PW}_{11}\text{Zn-APTES@SiO}_2$  as a heterogeneous catalyst for the oxidative desulfurization process (ODS) was investigated using a model oil containing dibenzothiophene (DBT, **ix** in Scheme 1) and 4,6-dimethyldibenzothiophene (4,6-DMDBT, **x** in Scheme 1). These ODS studies were performed in a biphasic system formed by equal amounts of the model oil and MeCN used as an extracting solvent. The ODS process of the model oil occurred in two distinct stages. The first corresponds to the initial extraction of the DBT and 4,6-DMDBT from the oil to the solvent by stirring the biphasic system for 10 min at 50 °C. After the initial extraction equilibrium has

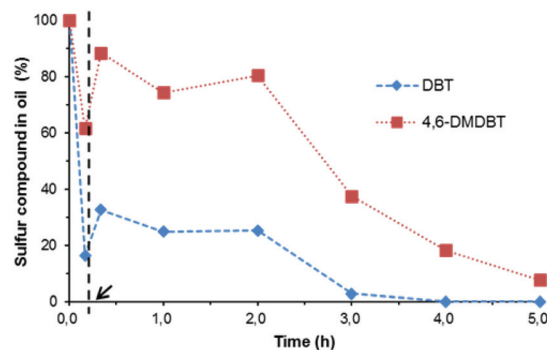


Fig. 8 Desulfurization of substrates showing the initial extraction stage (before the dashed line) and the catalytic stage (after the dashed line), at 50 °C.

been reached, the second step corresponds to the catalytic stage and it is started by the addition of the oxidant  $\text{H}_2\text{O}_2$ . In this stage, the sulfur refractory compounds (DBT and 4,6-DMDBT) were oxidized into sulfoxides and/or sulfones. These products remain in the MeCN phase since they are much more soluble in this organic polar phase than in the model oil. A blank reaction was performed using the same model oil and the same experimental conditions but in the absence of the catalyst  $\text{PW}_{11}\text{Zn-APTES@SiO}_2$ . In this case no oxidation of DBT or 4,6-DMDBT was detected.

Fig. 8 shows the results obtained for the desulfurization process of DBT and 4,6-DMDBT. For DBT the main extraction occurred in the initial extraction step, before addition of  $\text{H}_2\text{O}_2$ . After 10 min of stirring at 50 °C, 84% of the initial DBT in the model oil was extracted into the MeCN phase. A lower extraction yield (38%) was observed for 4,6-DMDBT. This distinct behavior between the two sulfur compounds can be caused by the higher solubility of the DBT in the MeCN and also by the steric hindrance of the methyl groups in 4 and 6 positions of 4,6-DMDBT that is expected to have a slower diffusion rate and thus a slower extraction.

After the addition of  $\text{H}_2\text{O}_2$ , the oxidation of DBT and 4,6-DMDBT occurred in the presence of  $\text{PW}_{11}\text{Zn-APTES@SiO}_2$ , probably in the MeCN phase since sulfones or sulfoxides were not detected in the oil phase. The consumption of non-oxidized DBT and 4,6-DMDBT in the extracting solvent leads to a continuous transfer of these compounds from the oil phase to the extracting phase. The desulfurization curves displayed in Fig. 8 demonstrate that after the addition of the oxidant, there is an induction period in the first 2 h. This behavior must be related with the mechanism of the ODS process, possibly with the formation of active catalytic species by interaction of the oxidant with the terminal bonds  $\text{W}^{\text{VI}}=\text{O}$  or with the substituted  $\text{Zn-OH}_2$  (water behaves as a labile ligand). This first step generates peroxy species that can then oxidize the sulfur compounds into sulfones and/or sulfoxides.<sup>66–68</sup> After 2 h, the efficiency of the ODS process catalyzed by  $\text{PW}_{11}\text{Zn-APTES@SiO}_2$  increases and a fast desulfurization is observed for DBT and 4,6-DMDBT. In fact, after 3 h, the model oil contained only 10 ppm of DBT and 56 ppm of 4,6-DMDBT. The oxidation

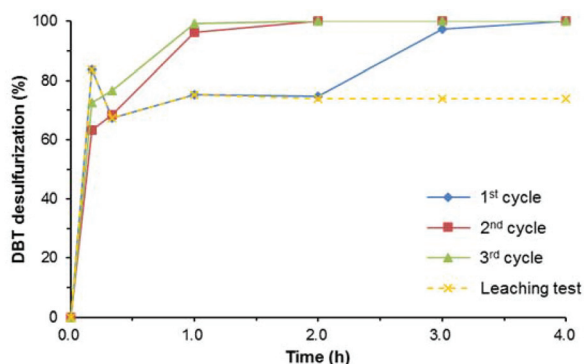


Fig. 9 Kinetic profile for DBT desulfurization for three consecutive ODS cycles, at 50 °C.

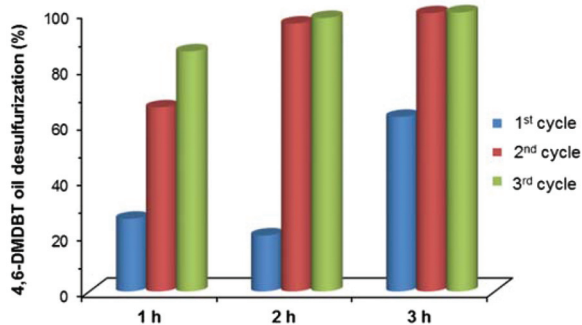


Fig. 10 Desulfurization data obtained for 4,6-DMDBT for three consecutive ODS cycles, at 50 °C.

of this last sulfur compound seems to be more difficult, possibly because its extraction from the model oil is slower than for DBT. This is corroborated by previous reports of a lower reactivity for the oxidation of 4,6-DMDBT than DBT. The difference in reactivity has been explained by the steric hindrance caused by the methyl groups in 4,6-DMDBT, hindering the interaction of this sulfur compound with active catalytic species and the oxidant.<sup>69–75</sup> Complete desulfurization of DBT was achieved after 4 h, while 4,6-DMDBT is near totally removed from oil after 5 h (Fig. 8).

The recyclability of the  $\text{PW}_{11}\text{Zn-APTES@SiO}_2$  was investigated for three consecutive ODS cycles. The solid catalyst was recovered after each ODS cycle by simple filtration followed by washing with MeCN, drying at room temperature, and then reutilization in a new ODS system under the same experimental conditions. Fig. 9 displays the kinetic profile of DBT desulfurization for the three consecutive cycles. It is possible to observe that the highest extraction of DBT from oil in consecutive cycles occurred during the initial extraction step. However, comparing the catalytic stage of the three ODS cycles, it is possible to notice that the induction period is only observed during the first cycle and a complete desulfurization of DBT is rapidly achieved for the consecutive cycles. In fact, the kinetic profile for DBT desulfurization is similar for the consecutive cycles and complete extraction of DBT is achieved

after 2 h, instead of the 3 h necessary during the first ODS cycle (Fig. 9).

Fig. 10 presents the desulfurization of 4,6-DMDBT for different ODS cycles at various reaction times. Also for this sulfur compound, the induction period observed during the first ODS cycle is not observed for the remaining cycles. Higher desulfurization is observed for 1, 2 and 3 h of reaction during the second and the third cycle, indicating that the catalyst is more active after the first cycle. This is probably explained by some modification of the initial composite into a more active catalytic composite during the induction period of the first cycle. Apparently, this new active form is stable to washing and drying of the catalyst, so no further induction period occurs in subsequent cycles.

### Catalyst material stability

The integrity and structural stability of the  $\text{PW}_{11}\text{Zn-APTES@SiO}_2$  composite were evaluated by several techniques. The catalyst was recovered after an ODS catalytic cycle ( $\text{PW}_{11}\text{Zn-APTES@SiO}_2\text{-ac}$ , where ac stands for after catalysis) and was studied by vibrational spectroscopy (FT-IR and FT-Raman), elemental analyses,  $^{31}\text{P}$  MAS NMR and SEM/EDS. The vibrational spectroscopy data of the composite after catalysis (Fig. 1) still exhibit the main bands associated with the  $\text{PW}_{11}\text{Zn}$  stretching modes together with the bands assigned to the silica framework (in FT-IR) and APTES (in FT-Raman). A decrease in the intensity of the bands associated with the POM stretches is observed, which should be due to some leaching that may have occurred. This is more evident in the FT-Raman spectrum, where the relative intensity of the peaks associated with  $\nu_{\text{as}}(\text{W-O}_d)$  and  $\nu_{\text{s}}(\text{W-O}_d)$  vibrations is reduced after catalytic use. The elemental analysis results of  $\text{PW}_{11}\text{Zn-APTES@SiO}_2\text{-ac}$  indicate a POM loading of 0.093 mmol per 1 g of material. Such a value represents a leaching of only 6% of  $\text{PW}_{11}\text{Zn}$  after the ODS cycle. To investigate the identity of the leached species, the  $^{31}\text{P}$  NMR analysis was performed using the resulting solution after catalytic use. This liquid NMR spectrum is presented in Fig. S3 in ESI† and no phosphorus signal was detected. Furthermore, the catalytic activity of the leached species was investigated by removing the solid catalyst after the first hour of reaction and following the ODS system until 4 h. Fig. 9 shows that no catalytic desulfurization was achieved in the absence of the solid. This result indicates that 0.17  $\mu\text{mol}$  of the leached species are not catalytically active and do not present phosphorus in their structure.

Analyzing the solid catalyst  $\text{PW}_{11}\text{Zn-APTES@SiO}_2\text{-ac}$  after 4 h of ODS use by  $^{31}\text{P}$  MAS NMR (Fig. 2), the spectrum exhibits a single broad peak centred at 0.04 ppm. After catalysis, the  $\text{PW}_{11}\text{Zn}$  molecules seem to be distributed in a single chemical environment. As previously discussed, this environment should correspond to  $\text{PW}_{11}\text{Zn}$  units interacting with the inner silica surface. The  $^{31}\text{P}$  MAS NMR results suggest that the  $\text{PW}_{11}\text{Zn}$  fragments that were in more central positions and experiencing less interactions with silica (hence with similar chemical shifts to the “free”  $\text{PW}_{11}\text{Zn}$ ) have been displaced to positions closer to the inner silica interface after the ODS

cycle. The  $^{13}\text{C}$  CP/MAS NMR spectrum of the composite after catalytic use (Fig. 3) presents three main peaks assigned to the C3 (43 ppm), C2 (21 ppm) and C1 (9 ppm) carbon atoms of the aminopropyl group. The chemical shifts are nearly identical with the ones before catalysis, suggesting that the structure of the aminopropyl groups of APTES remains essentially unaffected after catalytic use. The smaller peaks observed in the spectrum are most likely due to the presence of solvent molecules (MeCN) along with DBT and 4,6-DMDBT oxidation products. The integrity of the composite was also evaluated by SEM/EDS (Fig. 4). The SEM images of  $\text{PW}_{11}\text{Zn-APTES@SiO}_2\text{-ac}$  show that no significant changes in the morphology were observed after catalysis. The EDS spectra before and after catalysis display identical profiles, indicating the existence of P, W and Zn from the POM, in addition to silicon from the silica matrix and APTES.

## Conclusions

Novel silica nanoparticles incorporating  $[\text{PW}_{11}\text{Zn}(\text{H}_2\text{O})\text{O}_{39}]^{5-}$  were successfully prepared by the initial formation of a cross-linked organic–inorganic core composed of the polyoxometalate and an amine-organosilane, followed by the formation of a silica shell through the hydrolysis of TEOS. The obtained  $\text{PW}_{11}\text{Zn-APTES@SiO}_2$  was characterized by several techniques, namely vibrational spectroscopy (FT-IR and FT-Raman),  $^{31}\text{P}$  MAS NMR spectroscopy, SEM and EDS. The results show that the material is formed by uniform silica nanoscale spheres with approximately 350 nm in diameter and containing the POM/APTES hybrid dispersed in the silica matrix. The nanocomposite proved to be a versatile and robust heterogeneous catalyst for the oxidation of various olefins and also for the oxidative desulfurization of a model oil, using  $\text{H}_2\text{O}_2$  as the oxidant and MeCN as the solvent. The comparison between the catalytic performances of the heterogeneous and homogeneous catalysts shows that, in general, the incorporation of the POM into the silica spheres has led to an enhancement of the catalytic activity. The stability and robustness of the heterogeneous catalyst could be confirmed by different catalytic tests and several characterization techniques. Following the promising results obtained in this work, other novel POM-supported silica composites will be prepared by the method herein described and tested in catalytic oxidations.

## Acknowledgements

The authors acknowledge the Fundação para a Ciência e a Tecnologia (FCT, MEC, Portugal) for their general financial support through the strategic projects Pest-C/EQB/LA0006/2011 (to Associated Laboratory REQUIMTE) and PESt-C/CTM/LA0025/2022 (Strategic Project – LA 25-2001/2012), the R&D project PTDC/EQU-EQU/121677/2010, the fellowship SFRH/BPD/73191/2010 (to CG), the Portuguese Nuclear Magnetic Resonance Network (PRNMR) and the research group of

Dr Isabel Gonçalves from CICECO Laboratory, University of Aveiro, Portugal.

## References

- M. T. Pope and A. Müller, *Polyoxometalate Chemistry From Topology via Self-Assembly to Applications*, Kluwer Academic, Dordrecht, 2002.
- R. Neumann, in *Modern Oxidation Methods*, ed. J.-E. Backvall, Wiley-VCH, Weinheim, 2004, p. 223.
- O. A. Kholdeeva, in *Heterogeneous Catalysis Research Progress*, ed. M. B. Gunther, Nova Science Publ., New York, 2008, p. 267.
- I. V. Kozhevnikov, *Chem. Rev.*, 1998, **98**, 171–198.
- C. L. Hill, *J. Mol. Catal. A: Chem.*, 2007, **262**, 2–6.
- C. W. Jones, *Applications of hydrogen peroxide and derivatives*, Royal Society of Chemistry, Cambridge, 1999.
- A. C. Estrada, I. C. M. S. Santos, M. M. Q. Simões, M. G. P. M. S. Neves, J. A. S. Cavaleiro and A. M. V. Cavaleiro, *Appl. Catal., A*, 2011, **392**, 28–35.
- J. Kasai, Y. Nakagawa, S. Uchida, K. Yamaguchi and N. Mizuno, *Chem. – Eur. J.*, 2006, **12**, 4176–4184.
- O. A. Kholdeeva, N. V. Maksimchuk and G. M. Maksimov, *Catal. Today*, 2010, **157**, 107–113.
- S. K. Jana, Y. Kubota and T. Tatsumi, *J. Catal.*, 2008, **255**, 40–47.
- P. A. Shringarpure and A. Patel, *Dalton Trans.*, 2010, **39**, 2615–2621.
- R. Zhang and C. Yang, *J. Mater. Chem.*, 2008, **18**, 2691–2703.
- Y. Guo, Y. Yang, C. Hu, C. Guo, E. Wang, Y. Zou and S. Feng, *J. Mater. Chem.*, 2002, **12**, 3046–3052.
- S. S. Balula, I. C. M. S. Santos, L. Cunha-Silva, A. P. Carvalho, J. Pires, C. Freire, J. A. S. Cavaleiro, B. de Castro and A. M. V. Cavaleiro, *Catal. Today*, 2013, **203**, 95–102.
- C. M. Granadeiro, A. D. S. Barbosa, P. Silva, F. A. Almeida Paz, V. K. Saini, J. Fires, B. de Castro, S. S. Balula and L. Cunha-Silva, *Appl. Catal., A*, 2013, **453**, 316–326.
- S. S. Balula, C. M. Granadeiro, A. D. S. Barbosa, I. C. M. S. Santos and L. Cunha-Silva, *Catal. Today*, 2013, **210**, 142–148.
- S. S. Balula, L. Cunha-Silva, I. C. M. S. Santos, A. C. Estrada, A. C. Fernandes, J. A. S. Cavaleiro, J. Pires, C. Freire and A. M. V. Cavaleiro, *New J. Chem.*, 2013, **37**, 2341–2350.
- V. N. Panchenko, I. Borbath, M. N. Timofeeva and S. Gobolos, *J. Mol. Catal. A: Chem.*, 2010, **319**, 119–125.
- N. M. Okun, T. M. Anderson and C. L. Hill, *J. Am. Chem. Soc.*, 2003, **125**, 3194–3195.
- N. M. Okun, T. M. Anderson and C. L. Hill, *J. Mol. Catal. A: Chem.*, 2003, **197**, 283–290.
- N. M. Okun, M. D. Ritorto, T. M. Anderson, R. P. Apkarian and C. L. Hill, *Chem. Mater.*, 2004, **16**, 2551–2558.

- 22 C. S. Neves, C. M. Granadeiro, L. Cunha-Silva, D. Ananias, S. Gago, G. Feio, P. A. Carvalho, P. Eaton, S. S. Balula and E. Pereira, *Eur. J. Inorg. Chem.*, 2013, 2877–2886.
- 23 M. S. S. Balula, H. I. S. Nogueira and A. M. V. Cavaleiro, in *Advanced Materials Forum Iii, Pts 1 and 2*, ed. P. M. Vilarinho, 2006, vol. 514–516, pp. 1206–1210.
- 24 C. M. Granadeiro, R. A. S. Ferreira, P. C. R. Soares-Santos, L. D. Carlos, T. Trindade and H. I. S. Nogueira, *J. Mater. Chem.*, 2010, **20**, 3313–3318.
- 25 J. L. C. Sousa, I. C. M. S. Santos, M. M. Q. Simões, J. A. S. Cavaleiro, H. I. S. Nogueira and A. M. V. Cavaleiro, *Catal. Commun.*, 2011, **12**, 459–463.
- 26 Y. Zhao, Y. Li, W. Li, Y. Wu and L. Wu, *Langmuir*, 2010, **26**, 18430–18436.
- 27 W. Qi, Y. Z. Wang, W. Li and L. X. Wu, *Chem. – Eur. J.*, 2010, **16**, 1068–1078.
- 28 S. S. Balula, I. C. M. S. Santos, L. Cunha-Silva, A. P. Carvalho, J. Pires, C. Freire, J. A. S. Cavaleiro, B. de Castro and A. M. V. Cavaleiro, *Catal. Today*, 2013, **203**, 95–102.
- 29 S. Ribeiro, A. D. S. Barbosa, A. C. Gomes, M. Pillinger, I. S. Goncalves, L. Cunha-Silva and S. S. Balula, *Fuel Process. Technol.*, 2013, **116**, 350–357.
- 30 S. Ribeiro, C. M. Granadeiro, P. Silva, F. A. Almeida Paz, F. F. de Biani, L. Cunha-Silva and S. S. Balula, *Catal. Sci. Technol.*, 2013, **3**, 2404–2414.
- 31 Z. Nadealian, V. Mirkhani, B. Yadollahi, M. Moghadam, S. Tangestaninejad and I. Mohammadpoor-Baltork, *J. Coord. Chem.*, 2012, **65**, 1071–1081.
- 32 B. J. S. Johnson and A. Stein, *Inorg. Chem.*, 2001, **40**, 801–808.
- 33 J. M. Derfe and M. M. Derfe, in *Encyclopedia of Chemical Technology Kirk-Orthmer*, ed. S. Maurice, Wiley, New York, 1978, vol. 22.
- 34 Y. Chen, S. Zhao and Y.-F. Song, *Appl. Catal., A*, 2013, **466**, 307–314.
- 35 Y. Liu, S. Liu, S. Liu, D. Liang, S. Li, Q. Tang, X. Wang, J. Miao, Z. Shi and Z. Zheng, *ChemCatChem*, 2013, **5**, 3086–3091.
- 36 X.-M. Yan, P. Mei, L. Xiong, L. Gao, Q. Yang and L. Gong, *Catal. Sci. Technol.*, 2013, **3**, 1985–1992.
- 37 Z. E. A. Abdalla and B. Li, *Chem. Eng. J.*, 2012, **200–202**, 113–121.
- 38 N. Mizuno, K. Yamaguchi and K. Kamata, *Coord. Chem. Rev.*, 2005, **249**, 1944–1956.
- 39 X. Luo and C. Yang, *Phys. Chem. Chem. Phys.*, 2011, **13**, 7892–7902.
- 40 R. C. Schroden, C. F. Blanford, B. J. Melde, B. J. S. Johnson and A. Stein, *Chem. Mater.*, 2001, **13**, 1074–1081.
- 41 C. Rocchiccioli-Deltcheff, M. Fournier, R. Franck and R. Thouvenot, *Inorg. Chem.*, 1983, **22**, 207–216.
- 42 Y. Guo, C. Hu, C. Jiang, Y. Yang, S. Jiang, X. Li and E. Wang, *J. Catal.*, 2003, **217**, 141–151.
- 43 M. Hiraoui, M. Guendouz, N. Lorrain, A. Moadhen, L. Haji and M. Oueslati, *Mater. Chem. Phys.*, 2011, **128**, 151–156.
- 44 R. S. Pryce and L. L. Hench, *J. Mater. Chem.*, 2004, **14**, 2303–2310.
- 45 A. Ghanbari-Siahkali, A. Philippou, J. Dwyer and M. W. Anderson, *Appl. Catal., A*, 2000, **192**, 57–69.
- 46 T.-h. Chang, *J. Chem. Soc., Faraday Trans.*, 1995, **91**, 375–379.
- 47 G. Férey, C. Mellot-Draznieks, C. Serre, F. Millange, J. Dutour, S. Surblé and I. Margiolaki, *Science*, 2005, **309**, 2040–2042.
- 48 F. Lefebvre, *J. Chem. Soc., Chem. Commun.*, 1992, 756–757.
- 49 M. R. Mello, D. Phanon, G. Q. Silveira, P. L. Llewellyn and C. M. Ronconi, *Microporous Mesoporous Mater.*, 2011, **143**, 174–179.
- 50 Z. Luan, J. A. Fournier, J. B. Wooten and D. E. Miser, *Microporous Mesoporous Mater.*, 2005, **83**, 150–158.
- 51 A. Bordoloi, N. T. Mathew, F. Lefebvre and S. B. Halligudi, *Microporous Mesoporous Mater.*, 2008, **115**, 345–355.
- 52 P. D. Young and J. M. Notestein, *ChemSusChem*, 2011, **4**, 1671–1678.
- 53 C. Aubry, G. Chottard, N. Platzter, J. M. Bregeault, R. Thouvenot, F. Chauveau, C. Huet and H. Ledon, *Inorg. Chem.*, 1991, **30**, 4409–4415.
- 54 A. C. Dengel, W. P. Griffith and B. C. Parkin, *J. Chem. Soc., Dalton Trans.*, 1993, 2683–2688.
- 55 I. C. M. S. Santos, M. M. Q. Simões, M. M. M. S. Pereira, R. R. L. Martins, M. G. P. M. S. Neves, J. A. S. Cavaleiro and A. M. V. Cavaleiro, *J. Mol. Catal. A: Chem.*, 2003, **195**, 253–262.
- 56 J. Hu, K. Li, W. Li, F. Ma and Y. Guo, *Appl. Catal., A*, 2009, **364**, 211–220.
- 57 E. Poli, R. De Sousa, F. Jerome, Y. Pouilloux and J.-M. Clacens, *Catal. Sci. Technol.*, 2012, **2**, 910–914.
- 58 P. Shringarpure and A. Patel, *React. Kinet. Mech. Catal.*, 2011, **103**, 165–180.
- 59 J. Tang, X.-L. Yang, X.-W. Zhang, M. Wang and C.-D. Wu, *Dalton Trans.*, 2010, **39**, 3396–3399.
- 60 M. R. Maurya, P. Saini, C. Haldar and F. Avecilla, *Polyhedron*, 2012, **31**, 710–720.
- 61 C. M. Granadeiro, P. Silva, V. K. Saini, F. A. A. Paz, J. Pires, L. Cunha-Silva and S. S. Balula, *Catal. Today*, 2013, **218–219**, 35–42.
- 62 P. A. Shringarpure and A. Patel, *Chem. Eng. J.*, 2011, **173**, 612–619.
- 63 S. Pathan and A. Patel, *Dalton Trans.*, 2011, **40**, 348–355.
- 64 N. K. K. Raj, S. S. Deshpande, R. H. Ingle, T. Raja and P. Manikandan, *Catal. Lett.*, 2004, **98**, 217–223.
- 65 X. Yu, L. Xu, X. Yang, Y. Guo, K. Li, J. Hu, W. Li, F. Ma and Y. Guo, *Appl. Surf. Sci.*, 2008, **254**, 4444–4451.
- 66 H. Li, X. Jiang, W. Zhu, J. Lu, H. Shu and Y. Yan, *Ind. Eng. Chem. Res.*, 2009, **48**, 9034–9039.
- 67 Y. Ding, W. Zhu, H. Li, W. Jiang, M. Zhang, Y. Duan and Y. Chang, *Green Chem.*, 2011, **13**, 1210–1216.
- 68 X. Xue, W. Zhao, B. Ma and Y. Ding, *Catal. Commun.*, 2012, **29**, 73–76.
- 69 C. Komintarachat and W. Trakarnpruk, *Ind. Eng. Chem. Res.*, 2006, **45**, 1853–1856.

- 70 M. Te, C. Fairbridge and Z. Ring, *Appl. Catal., A*, 2001, **219**, 267–280.
- 71 X. Jiang, H. Li, W. Zhu, L. He, H. Shu and J. Lu, *Fuel*, 2009, **88**, 431–436.
- 72 M. A. Rezvani, A. F. Shojaie and M. H. Loghmani, *Catal. Commun.*, 2012, **25**, 36–40.
- 73 W. Zhu, W. Huang, H. Li, M. Zhang, W. Jiang, G. Chen and C. Han, *Fuel Process. Technol.*, 2011, **92**, 1842–1848.
- 74 J. H. Xu, S. Zhao, W. Chen, M. Wang and Y. F. Song, *Chem. – Eur. J.*, 2012, **18**, 4775–4781.
- 75 W. Trakarnpruk and K. Rujiraworawut, *Fuel Process. Technol.*, 2009, **90**, 411–414.